

# VARIABLE CATASTROPHIC DISRUPTION CRITERIA DURING PLANET FORMATION.

S. T. Stewart<sup>1</sup>, Z. M. Leinhardt<sup>2</sup>, <sup>1</sup>Harvard University, Department of Earth and Planetary Sciences, 20 Oxford St., Cambridge, MA 02138, U.S.A. (sstewart@eps.harvard.edu), <sup>2</sup>Department of Applied Math and Theoretical Physics, Cambridge University, CB3 0WA, U.K.

**Introduction:** Models for the collisional growth of planets center on criteria for coagulation and fragmentation. Recently, more sophisticated models have combined the collisional evolution of a population of bodies with their dynamical evolution [1-4]. Detailed understanding of the coupled collisional and dynamical processes has the power to unveil the history of the solar system, especially through the study of remnant populations of planetesimals.

Laboratory and numerical studies of fragmentation and the criteria for catastrophic disruption ( $Q_d^*$ , the energy per unit mass of the target delivered by the projectile such that half the target mass remains) have generally focused on nonporous, homogeneous materials, e.g., [5, 6]. Simulations of planet formation have implemented simplified rules, based on these studies, which govern the outcome of collisions. However, we expect significant changes in  $Q_d^*$  as (1) the collision velocities increase from subsonic to supersonic (>100 to 1000 m/s) encounters; (2) initially porous (and icy) planetesimals compact (and melt) into solid (homogeneous or layered/differentiated) planetesimals; and (3) solid bodies are disrupted into rubble piles. Each case results in a change of the coupling of the projectile's energy into the target and alters the value of  $Q_d^*$ . Furthermore, the sensitivity to these effects may vary between the strength-dominated and gravity-dominated size regimes [7] (Fig. 1).

Here, we explore the possible range of variability in disruption criteria under conditions expected during planet formation.

**Method:** We conduct numerical experiments of catastrophic disruption in the gravity regime and consider published laboratory fragmentation experiments in the strength regime. Supersonic collisions are modeled using a hybrid shock hydrocode (CTH [8]) to  $N$ -body gravity code (pkdgrav [9]) technique [10]. The supersonic collisions are normal impacts onto nonporous basalt targets, which have a range of material strength. Target radii range from 1 to 50 km, and projectile masses are much less than target masses.

Subsonic collisions are modeled exclusively with pkdgrav [11, 12]. Targets are gravitational aggregates of rigid spheres, with a bulk density range of 1.5 to 2.3 g cm<sup>-3</sup>, to represent rubble piles. Inelastic collisions between spheres are governed by a normal restitution

coefficient of 0.5 to 0.8 and no surface friction [13]. Because simulations of planet formation typically begin with a population of km-size bodies, we consider collisions between equal mass bodies with radii of 1, 10, and 50 km. The impact angle is 90°, producing  $Q_d^*$  values ~10% less than 45° impacts [6, 12].

**Results and Discussion.** The laboratory and numerical experiments are summarized in Fig. 1. Curves are the results from numerical experiments of supersonic [6] and subsonic collisions [11, 14]. Shaded region represents several supersonic numerical studies and theory [10, 15].

In the strength regime,  $Q_d^*$  is controlled primarily by the tensile strength of the material, which decreases with size for a brittle solid [16] (note the granite data [17]). For example, solid rocks have a larger  $Q_d^*$  than solid ice. In contrast, supersonic experiments in porous ice and sintered glass aggregates, which are mechanically weak, require a larger  $Q_d^*$  than their mechanically stronger, solid counterparts. Porous materials are efficient shock absorbers, and the projectile energy is inefficiently coupled to the target, requiring larger impact energies for disruption. However, in the subsonic regime, numerical [14] and laboratory experiments (▲ [18]) demonstrate that porous materials require lower disruption energies than a solid. In this case, the energy coupling is more efficient because of a combination of larger projectile sizes and less energy spent in material deformation (e.g., melting); hence, the tensile strength again governs the outcome. Note that subsonic and supersonic sintered glass aggregate experiments have overlapping mechanical strengths, but  $Q_d^*$  varies by >4 orders of magnitude [18, 19]!

In the gravity regime, the calculated range of  $Q_d^*$  depends primarily on the density and impact velocity [16]. As expected, the pkdgrav results follow an energy scaling power law,  $Q_d^* = aR_t^b$ , with  $b = 2$ . For  $\rho = 1.5 \text{ g cm}^{-3}$ ,  $a = 10^{-4.82}$ . Because energy coupling is less efficient in hypervelocity impacts,  $b$  is less than 2 and generally around 1.3. Under pure energy scaling, there is no dependence on the mass ratio of the target to projectile. For equal mass  $\rho = 1.5 \text{ g cm}^{-3}$  rubble piles, the critical encounter velocity for disruption is 5 m/s at 1 km and 270 m/s at 50 km. At larger target

sizes, the critical velocities transition into the supersonic regime.

We also consider the transition from catastrophic disruption to the cratering and accretion regimes. The normalized size of the largest fragment scales linearly with the normalized impact energy over an extremely wide range of impact conditions [6, 10, 11] (Fig. 2). The fragment mass is much more sensitive to impact energy in the subsonic regime compared to the supersonic regime, and there is a rapid transition from accretion to erosion. The critical encounter energies for accretion versus erosion are within a factor of two. Supersonic collisions transition into the crater regime at low energies, and subsonic collisions transition to a rebounding regime.

**Conclusions.** The catastrophic disruption criteria for bodies smaller than ~100 km changes dramatically during the formation and evolution of the solar system. Planet formation and collisional evolution calculations should implement velocity and porosity dependent criteria for disruption and fragmentation.

**References.** [1] Bottke, W.F., et al. (2005) *Icarus* **175**(1), 111-140. [2] Bottke, W.F., et al. (2005) *Icarus* **179**(1), 63-94. [3] Charnoz, S. and A. Morbidelli (2007) *Icarus* **188**(2), 468-480. [4] Bromley, B.C. and S.J. Kenyon (2006) *AJ* **131**(5), 2737-2748. [5] Holsapple, K.A. (1994) *Planet. Space Sci.* **42**(12), 1067-1078. [6] Benz, W. and E. Asphaug (1999) *Icarus* **142**(1), 5-20. [7] Leinhardt, Z.M., S.T. Stewart, and P.H. Schultz (2008) *The Solar System Beyond Neptune*, U. Arizona Press. [8] McGlaun, J.M., S.L. Thompson, and M.G. Elrick (1990) *Int. J. Impact Eng.* **10**, 351-360. [9] Richardson, D.C., et al. (2000) *Icarus* **143**, 45-59. [10] Leinhardt, Z.M. and S.T. Stewart (submitted) *Icarus*. [11] Stewart, S.T. and Z.M. Leinhardt (in prep.) *ApJ*

*Lett.* [12] Leinhardt, Z.M., D.C. Richardson, and T. Quinn (2000) *Icarus* **146**(1), 133-151. [13] Chau, K.T., R.H.C. Wong, and J.J. Wu (2002) *Int. J. Rock Mech. Min. Sci.* **39**(1), 69-77. [14] Benz, W. (2000) *Space Science Reviews* **92**(1-2), 279-294. [15] Melosh, H.J. and E.V. Ryan (1997) *Icarus* **129**(2), 562-564. [16] Housen, K.R. and K.A. Holsapple (1990) *Icarus* **84**(1), 226-253. [17] Housen, K.R. and K.A. Holsapple (1999) *Icarus* **142**(1), 21-33. [18] Setoh, M., et al. (2007) *Earth Planets Space* **59**(4), 319-324. [19] Love, S.G., F. Hörz, and D.E. Brownlee (1993) *Icarus* **105**, 216-224.

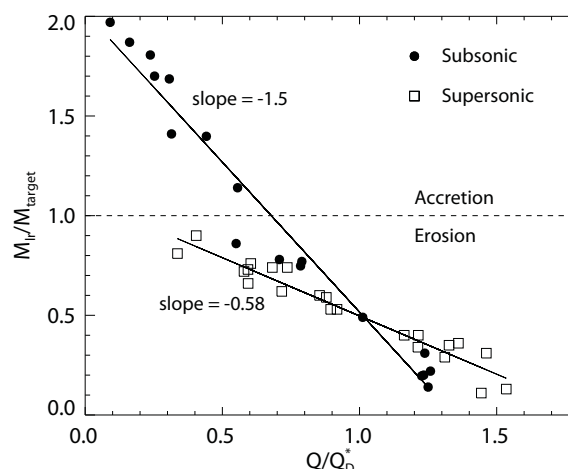


**Figure 2.** Mass of largest fragment normalized to target mass vs. impact energy normalized to catastrophic disruption energy for subsonic and supersonic collisions. Supersonic data for nonporous basalt targets [10]. Subsonic data for pkdgrav rubble piles [11].

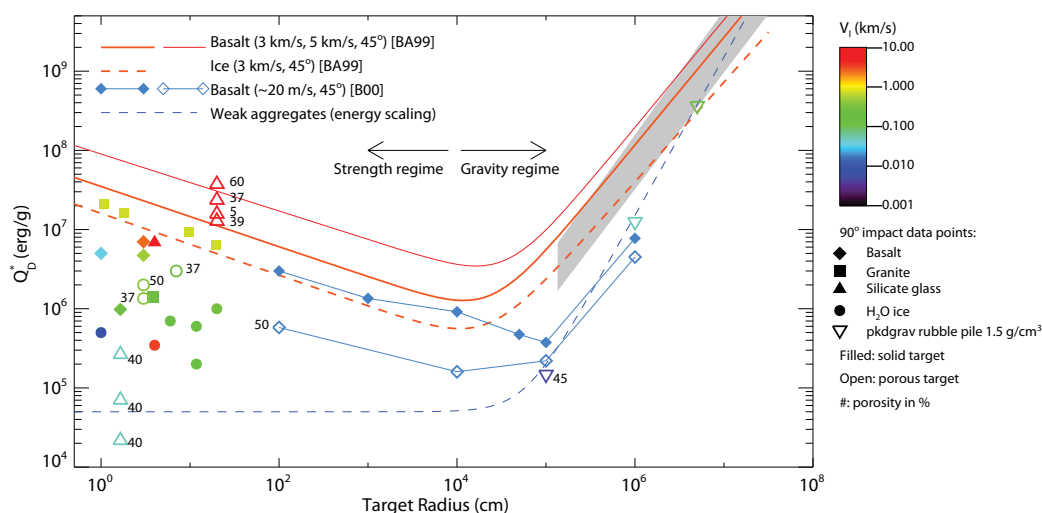


**Figure 1.** Laboratory (points with  $R_T < 1$  m) and numerical (lines) experiments on the criteria for catastrophic disruption and dispersal of half the target mass ( $Q_D^*$ ). Symbol and # indicate target material type and porosity. Color represents projectile velocity. References for all data points in [11].